Estimating regional fluxes of CO2 and CH4 using space-borne observations of XCH4

Atmos. Chem. Phys. Discuss., 14, 15867–15894, 2014
www.atmos-chem-phys-discuss.net/14/15867/2014/
doi:10.5194/acpd-14-15867-2014

Atmospheric Chemistry and Physics Discussions

Estimating regional fluxes of CO_2 and CH_4 using space-borne observations of $XCH_4 : XCO_2$

A. Fraser[1], P. I. Palmer[1], L. Feng[1], H. Bösch[2], R. Parker[2], E. J. Dlugokencky[3], P. B. Krummel[4], and R. L. Langenfelds[4]

[1]School of GeoSciences, University of Edinburgh, UK
[2]Department of Physics and Astronomy, University of Leicester, Leicester, UK
[3]US National Oceanic and Atmospheric Administration, Global Monitoring Division, Earth System Research Laboratory, Boulder, Colorado, USA
[4]Centre for Australian Weather and Climate Research, CSIRO Marine and Atmospheric Research, Aspendale, Victoria, Australia

Received: 23 May 2014 – Accepted: 6 June 2014 – Published: 17 June 2014

Correspondence to: P. I. Palmer (paul.palmer@ed.ac.uk)

Published by Copernicus Publications on behalf of the European Geosciences Union.

Abstract

We use the GEOS-Chem global 3-D atmospheric chemistry transport model to interpret $XCH_4 : XCO_2$ column ratios retrieved using a proxy method from the Japanese Greenhouse gases Observing SATellite (GOSAT). The advantage of these data over CO_2 and CH_4 columns retrieved independently using a full physics optimal estimation algorithm is that they suffer less from scattering-related regional bias. We show the model is able to reproduce observed global and regional spatial (mean bias = 0.7 %) and temporal variations (global $r^2 = 0.92$) of this ratio with model bias < 2.5 %. We also show these variations are driven by emissions of CO_2 and CH_4 that are typically six months out of phase which may reduce the sensitivity of the ratio to changes in either gas. To simultaneously estimate fluxes of CO_2 and CH_4 we use a formal Bayesian inverse model infrastructure. We use two approaches to independently resolve flux estimates of these two gases using GOSAT observations of $XCH_4 : XCO_2$: (1) the a priori error covariance between CO_2 and CH_4 describing common source from biomass burning; and (2) also fitting independent surface atmospheric measurements of CH_4 and CO_2 mole fraction that provide additional constraints, improving the effectiveness of the observed GOSAT ratio to constrain fluxes. We demonstrate the impact of these two approaches using Observing System Simulation Experiments. A posteriori flux estimates inferred using only the GOSAT ratios and taking advantage of the error covariance due to biomass burning are not consistent with the true fluxes in our experiments, as the inversion system cannot judge which species' fluxes to adjust. This can result in a posteriori fluxes that are further from the truth than the a priori fluxes. We find that adding the surface data to the inversion dramatically improves the ability of the GOSAT ratios to infer both CH_4 and CO_2 fluxes. We show that using real GOSAT $XCH_4 : XCO_2$ ratios together with the surface data during 2010 outcompetes inversions using the individual XCH_4 or the full-physics XCO_2 data products. Regional fluxes that show the greatest improvements have model minus observation differences with a large seasonal cycle such as Tropical South America for which we report a small but significant

ACPD
14, 15867–15894, 2014

annual source of CO_2 compared to a small annual sink inferred from the XCO_2 data. Based on our analysis we argue that using the ratios we may be reaching the limitations on the precision of these data.

1 Introduction

Space-borne atmospheric column measurements of CO_2 and CH_4 have the potential to improve our quantitative understanding of their surface fluxes and to underpin the development of testable climate policies. For these data to address these potential applications the column measurements have to meet strict precision requirements, reflecting small signals from surface fluxes (a few percent of the column amount) compared to the variations due to atmospheric transport. Any uncharacterized systematic error in these measurements compromises the ability of these data to infer surface fluxes. The CO_2 inverse problem is particularly sensitive to these systematic errors acting on length scales 10^3–10^4 km, in between the spatial scales of numerical models and those observed by the sparse network of well characterized upward-looking Fourier transform spectrometers, regional aircraft, and the network of ground-based measurements. Here, we develop a method to infer simultaneous regional CO_2 and CH_4 flux estimates (Fig. 1) from $XCH_4 : XCO_2$ ratios, retrieved from the Japanese Greenhouse gases Observing SATellite (GOSAT) using the proxy approach (based on University of Leicester proxy XCH_4 v4.0), which are less prone to systematic error from aerosols (Schepers et al., 2012).

Two methods have been used to retrieve CO_2 and CH_4 columns from calibrated GOSAT L1B spectra: the "full physics" and the "proxy" methods (Cogan et al., 2012; Parker et al., 2011). The full physics method uses an optimal estimation approach and incorporates a rigorous treatment of the atmospheric radiative transfer including the effects of clouds and aerosols. This method uses optimized spectral windows to fit CO_2 and CH_4. The main advantage of this approach is the error characterization of the a posteriori state vector, and the main disadvantage is having to accurately character-

ACPD
14, 15867–15894, 2014

ize the atmospheric aerosol for the radiative transfer calculation. The proxy method, used to infer CH_4 columns, fits both gases in nearby spectral windows with the assumption that any fitting artefacts common to both gases (e.g. aerosol and clouds) will be removed by taking the ratio of the two gases. This method is simpler than the full physics approach and more robust against scattering and as a result many more retrievals are possible from the GOSAT spectra. We also believe that these measurements are less compromised by systematic errors on regional scales. Interpretation of this ratio has in the past relied on scaling it with a model CO_2 column so that any erroneous model information about CO_2 can influence the interpretation of the GOSAT CH_4 columns (e.g. Parker et al., 2011; Fraser et al., 2013). We propose a method to simultaneously optimize CH_4 and CO_2 fluxes using the retrieved $XCH_4 : XCO_2$ ratio. This eliminates the need for a CO_2 model, removing the impact of model uncertainty on the retrieved methane columns, and increases the number of observations available to constrain CO_2 fluxes (Fig. 2).

In the following section we describe the space-borne and ground-based data used in our experiments. In Sect. 3 we describe the GEOS-Chem chemical transport model, and the data assimilation scheme developed for this work. In Sect. 4 we report the GOSAT and model spatial and temporal distributions of $XCH_4 : XCO_2$ ratios (Sect. 4.1), we test the assimilation scheme using a series of Observing System Simulation Experiments (OSSEs, Sect. 4.2) and present inversion results (Sect. 4.3). We conclude the paper in Sect. 5.

2 Data

2.1 GOSAT CO_2 and CH_4 atmospheric column mole fraction measurements

GOSAT was launched in 2009 by the Japanese Space Agency in a sun-synchronous orbit with an equatorial local overpass time of 13:00 LT, providing global coverage every three days (Kuze et al., 2009). GOSAT includes two instruments: TANSO-FTS (Thermal

ACPD
14, 15867–15894, 2014

and Near Infrared Sensor for carbon Observations – Fourier Transform Spectrometer) and TANSO-CAI (TANSO – Cloud and Aerosol Imager). The TANSO-FTS instrument provides short-wave infrared (SWIR) radiances from which dry-air mole fraction observations of CO_2 and CH_4, XCO_2 and XCH_4, can be retrieved.

We provide a brief description of the proxy retrieval algorithm used for XCO_2 and XCH_4 and refer the reader to a detailed description (Parker et al., 2011). XCH_4 and XCO_2 are retrieved at 1.65 µm and 1.61 µm, respectively. Past work has used this approach to infer observations of XCH_4 by scaling it by XCO_2, using XCO_2 as a proxy for the light path through the atmosphere. The mole fraction of XCH_4 is then obtained using a model estimate for XCO_2: ${XCH_4}^{PROXY} = \left[\frac{XCH_4}{XCO_2}\right]^{GOSAT} \times {XCO_2}^{MODEL}$, but using an inaccurate model of atmospheric CO_2 will introduce erroneous variability and bias in resulting values for ${XCH_4}^{PROXY}$. In this work we use the ratio $\left[\frac{XCH_4}{XCO_2}\right]^{GOSAT}$ directly, removing the requirement of model CO_2. We filter ratio values using cloud-screening and quality-of-fit filters recommended by Parker et al. (2011), and we further filter data with a solar zenith angle $> 70^{\circ}$, poleward of 60° latitude, or taken at medium gain (Fraser et al., 2013); the analysis of proxy XCH_4 reported by Fraser et al. (2013) used the previous version of the data. Figure 2 shows that the proxy method typically provides twice the number of observations available from the full physics approach.

2.2 In situ surface atmosphere mole fraction measurements

As described in Sect. 4.2, we use these data as independent constraints for CH_4 and CO_2 emission estimates, improving the ability of the GOSAT proxy ratio to act as a constraint on both CH_4 and CO_2 flux estimates. We assimilate data from 45 sites of the NOAA Earth System Research Laboratory (ESRL), Global Monitoring Division, version 28 August 2013 (Dlugokencky et al., 2013); nine sites from the CSIRO Global Atmospheric Sampling Laboratory (GASLAB), released August 2013 (Francey et al., 1996); and two sites from Environment Canada's Greenhouse Gas Measurement Program

ACPD
14, 15867–15894, 2014

(EC), released August 2013 (Worthy et al., 2003). Weekly air samples from all three networks are collected from sites distributed globally and data are reported on the NOAA 2004 (CH_4, all networks) and WMO X2007 (CO_2, ESRL, CSIRO) or WMO X83 (CO_2, EC) mole fraction scales. Figure 1 shows the location of the sites used in this work. Three sites are in both the ESRL and GASLAB networks: Mauna Loa, Hawaii; Cape Grim, Tasmania; and the South Pole. Alert, Nunavut is in all three networks. At these sites we average the data from the available networks, leaving 51 individual sites.

3 Models

3.1 The GEOS-Chem transport model

We use version v9-01-03 of the GEOS-Chem global 3-D atmospheric chemistry transport model, driven by assimilated meteorological fields from the NASA Global Modeling and Assimilation Office (version 5), to interpret observed variations of GOSAT proxy ratio measurements. We use the GEOS-5 meteorology at a horizontal resolution of 4° (latitude) $\times$ 5° (longitude) with 47 vertical levels that span from the surface to the mesosphere, with typically 35 levels in the troposphere.

The CH_4 and CO_2 simulations are described and evaluated against correlative data in Fraser et al. (2011) and Feng et al. (2011), respectively. Table 1 and Fig. 3 show the global annual flux estimates and temporal distribution of CH_4 and CO_2 fluxes, respectively. The main atmospheric sink of CH_4 is the hydroxyl radical and is described in the troposphere by monthly mean 3-D fields generated by a full chemistry version of the model. Loss rates for methane in the stratosphere are adapted from a 2-D stratospheric model (Wang et al., 2004).

3.2 The MAP inverse model

We use an inverse model that finds the maximum a posteriori (MAP) solution (Rodgers, 2000) to simultaneously optimize the magnitude of the CH_4 and CO_2 flux estimates by

ACPD
14, 15867–15894, 2014

fitting the a priori emission estimates, via the GEOS-Chem model (described above) to observations of GOSAT $XCH_4 : XCO_2$ ratios and in situ CH_4 and/or CO_2 mole fraction measurements. The MAP solution $\hat{\boldsymbol{x}}$ and associated error covariance $\hat{\mathbf{S}}$ can be written as:

$$\hat{\boldsymbol{x}} = \boldsymbol{x}_a + \left(\mathbf{K}^T\mathbf{S}_\epsilon^{-1}\mathbf{K} + \mathbf{S}_a^{-1}\right)^{-1}\mathbf{K}^T\mathbf{S}_\epsilon^{-1}(\boldsymbol{y} - \mathbf{K}\boldsymbol{x}_a) \quad (1)$$

$$\hat{\mathbf{S}} = \left(\mathbf{K}^T\mathbf{S}_\epsilon^{-1}\mathbf{K} + \mathbf{S}_a^{-1}\right)^{-1}, \quad (2)$$

where $\boldsymbol{x}_a$ denotes the a priori vector, including a priori flux estimates of CO_2 and CH_4; $\boldsymbol{y}$ denotes the measurement vector, including the GOSAT $XCH_4 : XCO_2$ ratios and in situ CH_4 and/or CO_2 observations; $\mathbf{K}$ denotes the Jacobian matrix, describing the sensitivity of model atmospheric concentrations to changes in the surface fluxes; $\mathbf{S}_a$ denotes the a priori flux error covariance matrix; and $\mathbf{S}_\epsilon$ denotes the observation error covariance matrix. The superscripts T and −1 denote the matrix transpose and inverse operations, respectively.

For our implementation, $\boldsymbol{x}_a$ includes monthly CH_4 and CO_2 in 13 geographical regions (Fig. 1). We separate the fluxes into contributions from biomass burning, the biosphere, and anthropogenic activities. For CH_4, the biosphere includes contributions from wetlands, oceans, termites, hydrates, and the soil sink; and the anthropogenic activities include ruminant animals, coal mining, oil and natural gas production, landfills, and rice. For CO_2, the biosphere includes the land and ocean fluxes, and the anthropogenic activities include fossil fuel combustion. We optimize for the total flux from the global ice and ocean regions. The state vector has 840 elements made up of 11 continental regions including three sectors each for CO_2 and CH_4 for 12 months, and for ice and ocean regions for the two gases for the 12 months.

We construct $\mathbf{S}_a$ as a diagonal matrix with the elements being the square of the error in the a priori fluxes, which we assume to be 100 % for the biospheric fluxes and 50 % for the biomass burning and anthropogenic fluxes. We assume no temporal correlation between fluxes in the same region or sector. We generally assume no correlation

ACPD
14, 15867–15894, 2014

between CH_4 and CO_2 fluxes because they are not co-emitted, with the exception of biomass burning for which we include a region-specific correlation with a mean value of 0.8 following previous work (Palmer et al., 2006).

The measurement vector $\boldsymbol{y}$ includes a spatial and temporal average of GOSAT $XCH_4 : XCO_2$ ratio measurements. We average the data into monthly means for the $4^\circ \times 5^\circ$ grid boxes of GEOS-Chem, which ensures a reasonable number of measurements for each month and increases the signal to noise of the observed ratio, as described below. Estimates inferred using finer temporal and spatial bins tend to be noisier, largely reflecting changes in the measurement coverage from clouds and aerosols, but still produce consistent results shown here when they are averaged monthly and on the model grid. For some experiments, $\boldsymbol{y}$ also includes in situ surface measurements of CH_4 and/or CO_2.

We construct $\mathbf{S}_\epsilon$ as a diagonal matrix with the diagonal elements being the standard error of the mean measurement error. For GOSAT, we use the provided measurement error. For surface data the measurement error is the standard error of the monthly mean calculated from the observations made over that month (Fraser et al., 2013). When we average we sum these errors in quadrature. We also include a model transport error to each individual measurement error. For both the GOSAT ratio measurements and surface in situ data we describe this error as 0.25 % for $(X)CO_2$ (Feng et al., 2011) and 0.5 % for $(X)CH_4$ (Wang et al., 2004).

The Jacobian matrix, $\mathbf{K}$, is constructed from forward runs of the model where the fluxes in each region and for each sector are perturbed by 1 Gt for CO_2 or 1 Tg for CH_4. The model is then sampled at the time and location of the observations, smoothed using GOSAT averaging kernels, and these sensitivities are averaged into monthly and regional means.

ACPD
14, 15867–15894, 2014

4 Results

4.1 Forward modelling of GOSAT $XCH_4 : XCO_2$ ratios

Figure 3 shows that for many geographical regions CH_4 and CO_2 flux estimates are six months out of phase, reflecting seasonal changes in wetland emissions of CH_4 and terrestrial CO_2 fluxes. This may reduce the sensitivity of the ratio to variations in either gas.

Figure 4 shows the observed annual variability of the $XCH_4 : XCO_2$ ratio is due mainly to XCH_4 variations. Common features include the gradient in the interhemispheric ratio and localized features due to orography, e.g., the Himalayan mountain range. The GEOS-Chem model reproduces the spatial pattern of the GOSAT ratio observations within $\simeq 2.5\,\%$. The model has a negative bias over the tropics, which is largely due to model positive bias for XCO_2, as expected. This figure illustrates the demanding accuracy and precision requirements associated with this space-borne measurement if it is to become a useful constraint for carbon cycle science. The monthly variation of observed values, here shown as the 1-σ value expressed as a percentage about the annual mean, is smallest for the $XCH_4 : XCO_2$ ratios for which scattering and other biases are removed.

Figure 5 shows that the model can typically capture 70 % of the observed temporal variability of $XCH_4 : XCO_2$ over different geographical regions. Over most regions we find the model has a progressively larger negative bias, reflecting its overestimation of the CO_2 growth rate. The model generally agrees best with GOSAT in the Northern Hemisphere extra-tropics, and the worst over Tropical South America, where we know the model underestimates the CO_2 biological uptake. While XCH_4 variations determine the spatial distribution of the GOSAT $XCH_4 : XCO_2$ ratio, we find that XCO_2 determines its seasonal cycle. This is particularly noticeable over boreal regions and Europe, where the peak in the ratio in the second half of the year is a result of decreasing XCO_2 due to increased uptake from the biosphere.

ACPD
14, 15867–15894, 2014

Figure 5 also illustrates the importance of using the ratio instead of the contributory columns. Both XCH_4 and XCO_2 are too noisy (due to variations in the atmosphere and surface) by themselves but the observed variations cancel out in the ratio. It should be noted that the XCH_4 and XCO_2 plotted here are not the final data products from GOSAT, but the intermediary products from which the ratio is calculated. Comparing this figure to Fig. 5 in Cogan et al. (2012) and Fig. 3 in Parker et al. (2011) shows that the regional bias between GOSAT and the model is much smaller in the ratio than in the individual species. While GEOS-Chem tends to underestimate the GOSAT ratio, the bias is more or less consistent between regions, which is not the case for either XCO_2 or XCH_4.

4.2 Inverse modelling of GOSAT $XCH_4 : XCO_2$ ratios: OSSEs

We use OSSEs, realistic numerical experiments, to characterize the method we use to estimate simultaneously CO_2 and CH_4 regional fluxes from GOSAT $XCH_4 : XCO_2$ ratios. For all these experiments, we sample the model at the location of the clear-sky GOSAT observations, apply GOSAT averaging kernels, and add, as a minimum, random error based on actual GOSAT measurements. Similarly, we sample the model at the time and location of the surface observations and add characteristic random noise informed by the data.

We conducted four broad sets of OSSEs: (1) those that use only the GOSAT $XCH_4 : XCO_2$ ratios, (2) those that use the GOSAT data and in situ measurements of CH_4 and/or CO_2, (3) those that use the best setup from (2) and vary the a priori fluxes, and (4) as (3) but including regional bias.

Figure 6a and b shows the results from experimental set (1). First, we assume that the a priori fluxes equal the true fluxes, allowing us to assess the level of numerical noise in the closed-loop system. We find that after setting the a priori to the true fluxes there is only a small difference between a posteriori and true fluxes that is within the uncertainty of the a posteriori fluxes. We then assume that the a priori fluxes are 20 % higher than the truth, allowing us to assess the efficacy with which the synthetic obser-

ACPD
14, 15867–15894, 2014

vations can recover the true flux estimates. For this experiment the observing system reconciles the model minus observation difference by simultaneously changing the CH_4 and CO_2 fluxes that are not always within the a posteriori flux uncertainties, which we attribute to the fact that there is no additional information about allocating this difference to a particular gas.

Figure 6c–e shows results from experimental set (2). Adding either CH_4 or CO_2 surface observations to the measurement vector reduces the bias between the a posteriori and true fluxes, but also reduces the error reduction of the other species. We find that assimilating both CH_4 and CO_2 surface observations gives the smallest difference from the truth and the largest error reductions; we adopt this as our control experimental setup in the following sections. We accept the larger standard deviations as the fluxes are closer to the truth. For reference, using only the surface data returns error reductions of approximately 23 % for both species (not shown). Figure 7 shows the results from experimental set (3). This control observing system can return the true fluxes for a wide array of varying CH_4 and CO_2 fluxes for most geographical regions.

In experiment set (4) (not shown) we assess the impact of prescribed observation bias to the GOSAT data on the a posteriori flux estimates; assuming that the surface data is unbiased or at least can be identified readily via ongoing calibration/validation activities. We assume a latitudinally-varying bias, which was superimposed onto the "true" atmospheric measurements plus random error (0.005 ppb ppm^{-1}) for the monthly gridded measurement vector. To describe the latitudinal bias, we used a second-degree polynomial with a minimum at the South Pole and a maximum at the North Pole; our choice of this polynomial is based on the bias between the model and GOSAT data. This bias ranges from -0.08–0.06 ± 0.005 ppb ppm^{-1}. As part of the data preprocessing inverse model analysis, we either assume the data are unbiased or fit a latitudinally-varying bias. For our bias correction we fit a fourth-degree polynomial to the mean annual difference between the model and the data; we find that using higher degree polynomials did not significantly change our results. Not fitting for the bias results in CH_4 and CO_2 fluxes that are up to 10 Tg and 0.4 Gt different from the

ACPD
14, 15867–15894, 2014

true fluxes, respectively. Removing the bias in pre-processing returns values that are close to the true fluxes.

4.3 Analysis of GOSAT $XCH_4 : XCO_2$ ratios

Figure 8 and Table 2 show flux estimates inferred from GOSAT $XCH_4 : XCO_2$ data and surface mole fraction observations of CH_4 and CO_2 (Sect. 2), and independent flux estimates of CH_4 and CO_2 inferred using an ensemble Kalman filter (EnKF) from GOSAT XCH_4 proxy data (Fraser et al., 2013) and XCO_2 full physics data (Feng et al., 2011).

For CH_4, the general tendency of a posteriori fluxes, relative to a priori values, are consistent between the $XCH_4 : XCO_2$ ratio and the proxy XCH_4 data, but based on a posteriori uncertainties the magnitude of these fluxes can be statistically different. The ratio infers larger emissions from Tropical South America, Northern Africa, and Temperate Eurasia. Error reductions resulting from assimilating $XCH_4 : XCO_2$ ratio data are typically 30 % but can be up to 60 % (Temperate Eurasia). For some regions, the error reduction from using the ratio is larger from using the individual gas but for others the reduction is smaller. Geographical regions with notable improvements in our understanding from assimilating the ratio data include Tropical and Temperate South America, Northern Africa, and Temperate Eurasia. Strictly speaking we cannot compare directly the CH_4 flux estimated reported by Fraser et al. (2013) and those inferred from the $XCH_4 : XCO_2$ ratio data. As noted above we are using a newer version of the proxy retrieval that includes updated a priori information particularly for stratospheric CH_4 concentrations and updates to the retrieval grid and spectroscopic input, resulting in 5–10 % more clear-sky measurements; we are using a newer version of the GEOS-Chem transport model; and most importantly we treat the measurements differently, reflecting the difficulty in the small observed changes in the $XCH_4 : XCO_2$ ratio data.

For CO_2, a posteriori fluxes inferred from the GOSAT ratio can be statistically different to those inferred from the EnKF inversion, including Tropical South America, Southern Africa, Boreal Eurasia, Tropical Asia, and Australasia. These differences between the

ACPD
14, 15867–15894, 2014

inversion largely reflect the larger volume of $XCH_4 : XCO_2$ ratio data resulting in better spatial and temporal coverage (Fig. 2). We may also expect the largest differences where we believe there are the greatest biases in the other single gas retrievals. We find that the associated error reductions for the CO_2 fluxes inferred from the $XCH_4 : XCO_2$ ratio data are typically larger than those for CH_4, and are different from those inferred from the EnKF inversion.

5 Concluding remarks

We have interpreted measurements of $XCH_4 : XCO_2$ from GOSAT in which XCH_4 and XCO_2 are retrieved in nearby spectral windows under the assumption that their ratio will largely remove common sources of biases. By interpreting the ratio directly we minimize any bias introduced by model XCO_2; although we acknowledge other sources of model bias remain. A major advantage of the ratio is this data product does not suffer from the measurement bias that befalls the full physics XCO_2 data. Another advantage is that the volume of these data is greater than their full physics counterpart. While the ratio benefits from these three advantages the difference between model and observed quantities are much smaller (typically $< \pm 2\%$) than either XCO_2 or XCH_4 becoming comparable in magnitude to other sources of error, e.g. model transport error, that cannot easily be characterized and removed; by using the ratio we may be reaching the limitations on the precision of these data and our ability to interpret them using current-day transport models. However, over particular geographical regions we find there are seasonally varying GOSAT minus model ratio differences that are large enough to exploited, e.g., Tropical South America and Tropical Asia.

Using a series of numerical experiments we showed that the simultaneous estimation of CO_2 and CH_4 fluxes using the GOSAT ratio is possible with the information split as a function of the a priori uncertainties, however the inversion system returns unphysical fluxes in some regions. We showed that including surface mole fraction measurements of CO_2 and CH_4 in the measurement vector provides an "anchor" for the inversion, and

ACPD
14, 15867–15894, 2014

we showed that the combined GOSAT and surface data can distinguish between CO_2 and CH_4 fluxes.

Using real data for 2010 we showed that the combination of the GOSAT $XCH_4 : XCO_2$ ratio and the surface mole fraction data outcompeted inversions using the individual XCH_4 and XCO_2 GOSAT data and corresponding surface data. We found the greatest differences between the two approaches over the regions where we found that the GOSAT minus model difference had a seasonal variation that was larger than a few percent. For instance, we found that Tropical South America was a small but significant source of CO_2 while analysis of full physics XCO_2 showed a small sink term. Analysis of the ratio led to slightly larger reductions globally, and in some regions, primarily in the tropics, much larger reductions in uncertainty of CO_2 and CH_4.

The main reason for using the $XCH_4 : XCO_2$ ratio is that it minimizes scattering and potentially other biases and significantly increases geographical coverage. Although CO_2 and CH_4 do not share many common sources that result in significant atmospheric covariance we have shown that: (1) the combined information from these two gases can be disentangled using other data, and (2) the result is an improvement over what can be achieved using observations of either full-physics XCO_2 or XCH_4. Consequently, the use of space-borne observations of the $XCH_4 : XCO_2$ ratio will be of particular interest for estimating CO_2 surface fluxes over regions that are characterized by frequent cloud cover and high aerosol loading such as the tropics where the quality and coverage of full-physics XCO_2 retrieval approaches will be limited even for missions with spatial footprints smaller than GOSAT. This ratio approach could also be used in combination with other atmospheric tracers that help improve the source attribution of CO_2, e.g, carbon monoxide, where the ensuing correlation is driven by incomplete combustion (Palmer et al., 2006). Space-borne mission concept development related to the carbon cycle should not only focus on the primary compound but also on any secondary compound that will help interpret the observed variability of that primary gas.

ACPD
14, 15867–15894, 2014

Acknowledgements. We thank Doug Worthy for the Environment Canada data. NOAA ESRL is supported by NOAA's Climate Program Office; and CSIRO research at Cape Grim is supported by the Australian Bureau of Meteorology. AF and RP were supported by the Natural Environment Research Council National Centre for Earth Observation (NCEO). LF was partly funded by the "Data Assimilation Project-Interfacing EO data with atmospheric and land surface models" ESA contract 4000104980/1-LG. HB, RP and LF also acknowledge funding by the ESA Climate Change Initiative (GHG-CCI). PIP gratefully acknowledges his Royal Society Wolfson Research Merit Award.

References

Bloom, A. A., Palmer, P. I., Fraser, A., and Reay, D. S.: Seasonal variability of tropical wetland CH_4 emissions: the role of the methanogen-available carbon pool, Biogeosciences, 9, 2821–2830, doi:10.5194/bg-9-2821-2012, 2012. 15885

Cogan, A. J., Boesch, H., Parker, R. J., Feng, L., Palmer, P. I., Blavier, J.-F. L., Deutscher, N. M., Macatangay, R., Notholt, J., Roehl, C., Warneke, T., and Wunch, D.: Atmospheric carbon dioxide retrieved from the Greenhouse gases Observing SATellite (GOSAT): comparison with ground-based TCCON observations and GEOS-Chem model calculations, J. Geophys. Res., 117, D21301, doi:10.1029/2012JD018087, 2012. 15869, 15876

Dlugokencky, E. J., Lang, P. M., Crotwell, A., Masarie, K. A., and Crotwell, M.: Atmospheric methane dry air mole fractions from the NOAA ESRL carbon cycle cooperative global air sampling network, 1983–2012, Version: 2013-08-28, available at: ftp://aftp.cmdl.noaa.gov/data/trace_gases/ch4/flask/surface/ (last access: September 2013), 2013. 15871

Feng, L., Palmer, P. I., Yang, Y., Yantosca, R. M., Kawa, S. R., Paris, J.-D., Matsueda, H., and Machida, T.: Evaluating a 3-D transport model of atmospheric CO_2 using ground-based, aircraft, and space-borne data, Atmos. Chem. Phys., 11, 2789–2803, doi:10.5194/acp-11-2789-2011, 2011. 15872, 15874, 15878, 15886, 15894

Francey, R. J., Steele, L. P., Langenfelds, R. L., Lucarelli, M. P., Allison, C. E., Beardsmore, D. J., Coram, S. A., Derek, N., de Silva, F. R., Etheridge, D. M., Fraser, P. J., Henry, R. J., Turner, B., Welch, E. D., Spencer, D. A., and Cooper, L. N.: Global Atmospheric Sampling Laboratory (GASLAB): supporting and extending the Cape Grim trace gas programs, in: Baseline At-

ACPD
14, 15867–15894, 2014

mospheric Program (Australia), Bureau of Meteorology and CSIRO Division of Atmospheric Research, Melbourne, Australia, 8–29, 1996. 15871

Fraser, A., Chan Miller, C., Palmer, P. I., Deutscher, N. M., Jones, N. B., and Griffith, D. W. T.: The Australian methane budget: interpreting surface and train-borne measurements using a chemistry transport model, J Geophys. Res., 116, D20306, doi:10.1029/2011JD015964, 2011. 15872

Fraser, A., Palmer, P. I., Feng, L., Boesch, H., Cogan, A., Parker, R., Dlugokencky, E. J., Fraser, P. J., Krummel, P. B., Langenfelds, R. L., O'Doherty, S., Prinn, R. G., Steele, L. P., van der Schoot, M., and Weiss, R. F.: Estimating regional methane surface fluxes: the relative importance of surface and GOSAT mole fraction measurements, Atmos. Chem. Phys., 13, 5697–5713, doi:10.5194/acp-13-5697-2013, 2013. 15870, 15871, 15874, 15878, 15886, 15894

Fung, I., John, J., Lerner, J., Matthews, E., Prather, M., Steele, L. P., and Fraser, P. J.: Three-dimensional model synthesis of the global methane cycle, J. Geophys. Res., 96, 13033–13065, doi:10.1029/91JD01247, 1991. 15885

Gurney, K. R., Law, R. M., Denning, A. S., Rayner, P. J., Baker, D., Bousquet, P., Bruhwiler, L., Chen, Y.-H., Ciais, P., Fan, S., Fung, I. Y., Gloor, M., Heimann, M., Higuchi, K., John, J., Maki, T., Maksyutov, S., Masarie, K., Peylin, P., Prather, M., Pak, B. C., Randerson, J., Sarmiento, J., Taguchi, S., Takahashi, T., and Yuen, C.-W.: Towards robust regional estimates of CO_2 sources and sinks using atmospheric transport models, Nature, 415, 626–630, doi:10.1038/415626a, 2002. 15887

Houweling, S., Kaminski, T., Dentener, F., Lelieveld, J., and Heimann, M.: Inverse modeling of methane sources and sinks using the adjoint of a global transport model, J. Geophys. Res., 104, 26137–26160, doi:10.1029/1999JD900428, 1999. 15885

Kuze, A., Suto, H., Nakajima, M., and Hamazaki, T.: Thermal and near infrared sensor for carbon observation Fourier-transform spectrometer on the Greenhouse Gases Observing Satellite for greenhouse gases monitoring, Appl. Optics, 48, 6716–6733, doi:10.1364/AO.48.006716, 2009. 15870

Oda, T. and Maksyutov, S.: A very high-resolution (1 km × 1km) global fossil fuel CO_2 emission inventory derived using a point source database and satellite observations of nighttime lights, Atmos. Chem. Phys., 11, 543–556, doi:10.5194/acp-11-543-2011, 2011. 15885

Olivier, J. G. J., van Aardenne, J. A., Dentener, F., Ganzeveld, L., and Peters, J. A. H. W.: Recent trends in global greenhouse gas emissions: regional trends and spatial distribution of key

ACPD
14, 15867–15894, 2014

sources, in: Non-CO_2 Greenhouse Gases (NCGG-4), edited by: van Amstel, A., Millpress, Rotterdam, 325–330, 2005. 15885
Palmer, P., Suntharalingam, P., Jones, D., Jacob, D., Streets, D., Fu, Q., Vay, S., and Sachse, G.: Using CO_2 : CO correlations to improve inverse analyses of carbon fluxes, J. Geophys. Res., 111, D12318, doi:10.1029/2005JD006697, 2006. 15874, 15880
Parker, R., Boesch, H., Cogan, A., Fraser, A., Feng, L., Palmer, P. I., Messerschmidt, J., Deutscher, N., Griffith, D. W., Notholt, J., Wennberg, P. O., and Wunch, D.: Methane observations from the Greenhouse Gases Observing SATellite: comparison to ground-based TCCON data and model calculations, Geophys. Res. Lett., 38, L15807, doi:10.1029/2011GL047871, 2011. 15869, 15870, 15871, 15876
Randerson, J., Thompson, M., Conway, T., Fung, I., and Field, C.: The contribution of terrestrial sources and sinks to trends in the seasonal cycle of atmospheric carbon dioxide, Global Biogeochem. Cy., 11, 535–560, 1997. 15885
Rodgers, C. D.: Inverse Methods for Atmospheric Sounding: Theory and Practice, World Scientific Publishing, River Edge, NJ, 2000. 15872
Schepers, D., Guerlet, S., Butz, A., Landgraf, J., Frankenberg, C., Hasekamp, O., Blavier, J.-F., Deutscher, N. M., Griffith, D. W. T., Hase, F., Kyro, E., Morino, I., Sherlock, V., Sussmann, R., and Aben, I.: Methane retrievals from Greenhouse Gases Observing Satellite (GOSAT) shortwave infrared measurements: performance comparison of proxy and physics retrieval algorithms, J. Geophys. Res., 117, D10307, doi:10.1029/2012JD017549, 2012. 15869
Takahashi, T., Sutherland, S. C., Wanninkhof, R., Sweeney, C., Feely, R. A., Chipman, D. W., Hales, B., Friederich, G., Chavez, F., Sabine, C., Watson, A., Bakker, D. C., Schuster, U., Metzl, N., Yoshikawa-Inoue, H., Ishii, M., Midorikawa, T., Nojiri, Y., Körtzinger, A., Steinhoff, T., Hoppema, M., Olafsson, J., Arnarson, T. S., Tilbrook, B., Johannessen, T., Olsen, A., Bellerby, R., Wong, C., Delille, B., Bates, N., and de Baar, H. J.: Climatological mean and decadal change in surface ocean pCO_2, and net sea-air $\{CO_2\}$ flux over the global oceans, Deep-Sea Res. Pt. II, 56, 554–577, doi:10.1016/j.dsr2.2008.12.009, 2009. 15885
van der Werf, G. R., Randerson, J. T., Giglio, L., Collatz, G. J., Mu, M., Kasibhatla, P. S., Morton, D. C., DeFries, R. S., Jin, Y., and van Leeuwen, T. T.: Global fire emissions and the contribution of deforestation, savanna, forest, agricultural, and peat fires (1997–2009), Atmos. Chem. Phys., 10, 11707–11735, doi:10.5194/acp-10-11707-2010, 2010. 15885
Wang, J. S., Logan, J. A., McElroy, M. B., Duncan, B. N., Megretskaia, I. A., and Yantosca, R. M.: A 3-D model analysis of the slowdown and interannual variability in the methane growth

ACPD
14, 15867–15894, 2014

rate from 1988 to 1997, Global Biogeochem. Cy., 18, GB3011, doi:10.1029/2003GB002180, 2004. 15872, 15874

Worthy, D. E., Platt, J. A., Kessler, R., Ernst, M., and Racki, S.: The Greenhouse Gases Measurement Program, measurement procedures and data quality, in: Canadian Baseline Program; Summary of Progress to 2002, Meteorological Service of Canada, Quebec, 97–120, 2003. 15872

ACPD

14, 15867–15894, 2014

Table 1. A priori sources of carbon dioxide and methane used in the GEOS-Chem model for 2010.

CO_2	A priori magnitude ($Gt\,year^{-1}$)	Reference
Fossil fuel	14.8	ODIAC (Oda and Maksyutov, 2011)
Oceans	−5.2	Takahashi et al. (2009)
Biosphere	3.4	CASA (Randerson et al., 1997)
Biomass burning	8.6	GFEDv3 (van der Werf et al., 2010)
CH_4	A priori magnitude ($Tg\,year^{-1}$)	Reference
Ruminant animals	92.8	EDGAR 3.2 FT (Olivier et al., 2005)
Coal mining	47.1	EDGAR 3.2 FT (Olivier et al., 2005)
Oil and natural gas production	42.8	EDGAR 3.2 FT (Olivier et al., 2005)
Landfills	44.7	EDGAR 3.2 FT (Olivier et al., 2005)
Rice	68.0	Bloom et al. (2012)
Wetlands	192.0	Bloom et al. (2012)
Biomass burning	19.4	GFEDv3 (van der Werf et al., 2010)
Oceans	15.1	Houweling et al. (1999)
Termites	20.1	Fung et al. (1991)
Hydrates	5.0	Fung et al. (1991)
Soil Sink	−25.2	Fung et al. (1991)

ACPD
14, 15867–15894, 2014

Table 2. A priori and a posteriori CH_4 and CO_2 regional land fluxes and 1-σ uncertainties inferred from GOSAT $XCH_4 : XCO_2$ and in situ mole fraction measurements. Fluxes inferred from previous work (Fraser et al., 2013; Feng et al., 2011) using and ensemble Kalman Filter are denoted EnKF. CH_4 and CO_2 fluxes are reported as Tg CH_4 year^{-1} and Gt C year^{-1}, respectively.

	CH_4 Prior		CH_4 Posterior (this work)		CH_4 Posterior (EnKF)		CO_2 Prior		CO_2 Posterior (this work)		CO_2 Posterior (EnKF)	
Region	Flux	1-σ	Flux	1-σ	Flux	1-σ	Flux	1-σ	Flux	1-σ	Flux	1-σ
Boreal North America	4.1	1.0	4.0	0.9	4.8	0.9	−0.4	0.5	−0.7	0.3	0.1	0.1
Europe	44.5	3.6	31.3	2.4	39.8	2.3	0.5	0.8	0.6	0.4	0.6	0.2
Boreal Eurasia	15.2	2.5	19.3	1.9	15.0	2.5	−0.7	1.0	−1.5	0.9	−0.4	0.2
Temperate North America	58.5	4.1	62.5	3.6	64.9	3.1	0.9	0.8	1.2	0.5	1.4	0.2
Northern Africa	49.6	4.3	65.6	3.5	46.8	4.2	0.3	0.6	0.4	0.5	0.2	0.2
Temperate Eurasia	127.9	11.8	140.2	4.4	124.0	6.5	2.7	0.7	3.4	0.4	3.4	0.2
Tropical South America	45.1	5.6	59.0	3.1	51.1	4.1	−0.2	0.5	0.3	0.3	−0.3	0.3
Tropical Asia	34.6	4.5	40.6	3.2	42.9	3.1	0.7	0.2	0.9	0.2	1.5	0.2
Temperate South America	60.5	5.8	50.9	3.3	55.8	5.6	−0.4	0.6	−0.6	0.4	−0.5	0.3
Southern Africa	46.0	5.1	43.6	3.6	41.4	3.1	−1.4	0.8	−1.9	0.6	0.1	0.2
Australasia	16.7	1.4	17.9	1.3	17.8	1.3	−0.1	0.2	−0.4	0.2	0.7	0.2

ACPD
14, 15867–15894, 2014

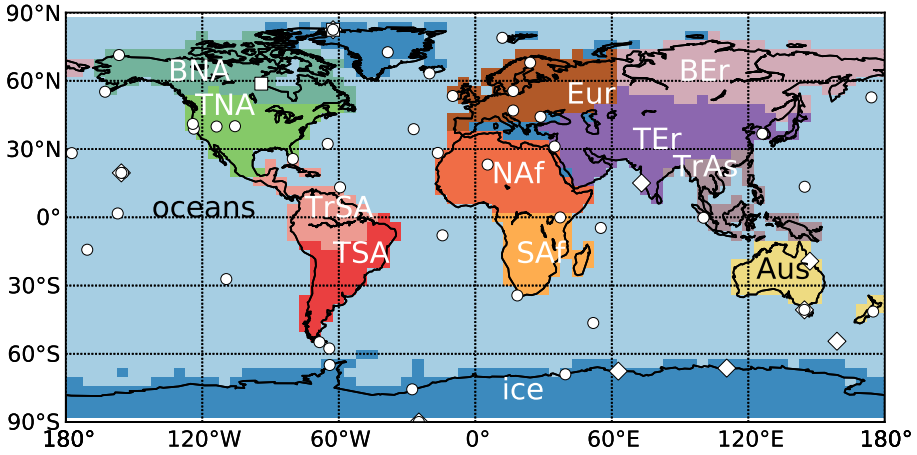

Figure 1. Distribution of the 13 geographical regions for which we estimate CO_2 and CH_4 fluxes, and the location of 57 co-operative flask sampling sites with data covering the study period, January–December 2010. The land regions, informed by previous work (Gurney et al., 2002) include: Boreal North America (BNA), Temperate North America (TNA), Tropical South America (TrSA), Temperate South America (TSA), Northern Africa (NAf), Southern Africa (SAf), Boreal Eurasia (BEr), Temperate Eurasia (TEr), Tropical Asia (TrAs), Australasia (Aus), and Europe (Eur). The ground-based measurement sites run by NOAA ESRL, CSIRO GASLAB, and EC are denoted by white circles, white diamonds, and white squares, respectively.

ACPD
14, 15867–15894, 2014

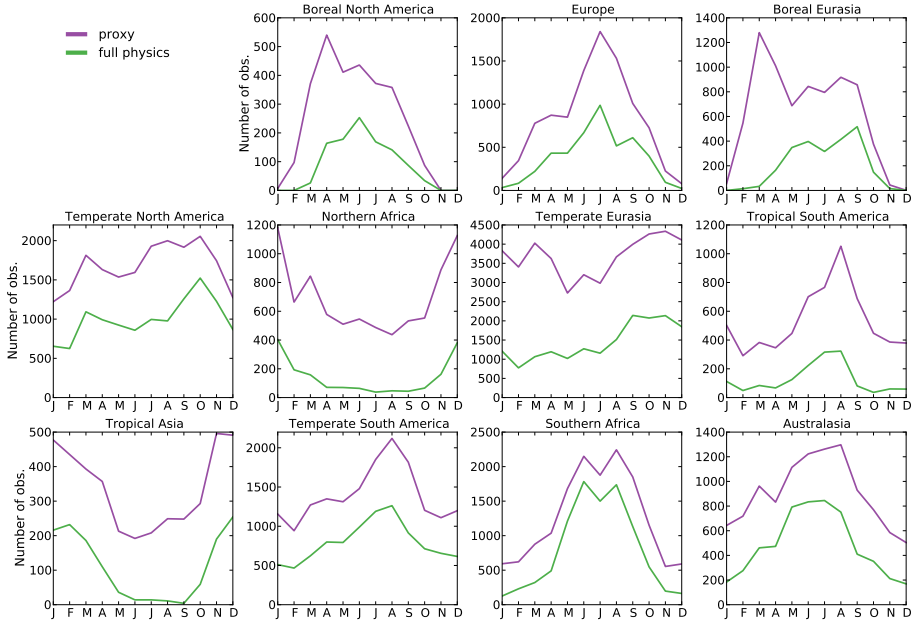

Figure 2. The number of GOSAT observations available per month during 2010 over specific geographical regions (Fig. 1) from the full-physics and proxy retrieval algorithms.

ACPD
14, 15867–15894, 2014

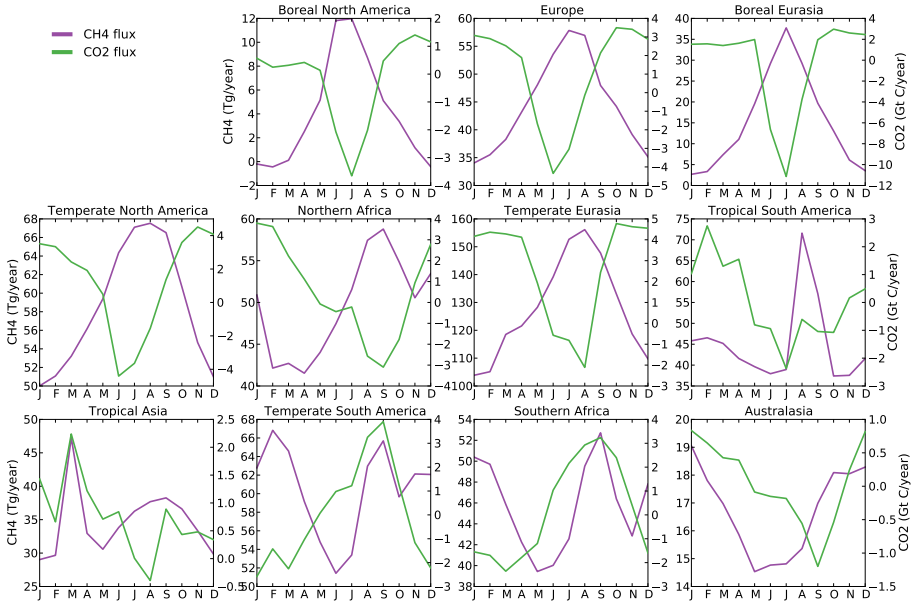

Figure 3. Monthly a priori emissions for CH_4 (Tg CH_4 year^{-1}) and CO_2 (Gt C year^{-1}) for the land regions shown in Fig. 1. Note the different *y*-scales.

ACPD
14, 15867–15894, 2014

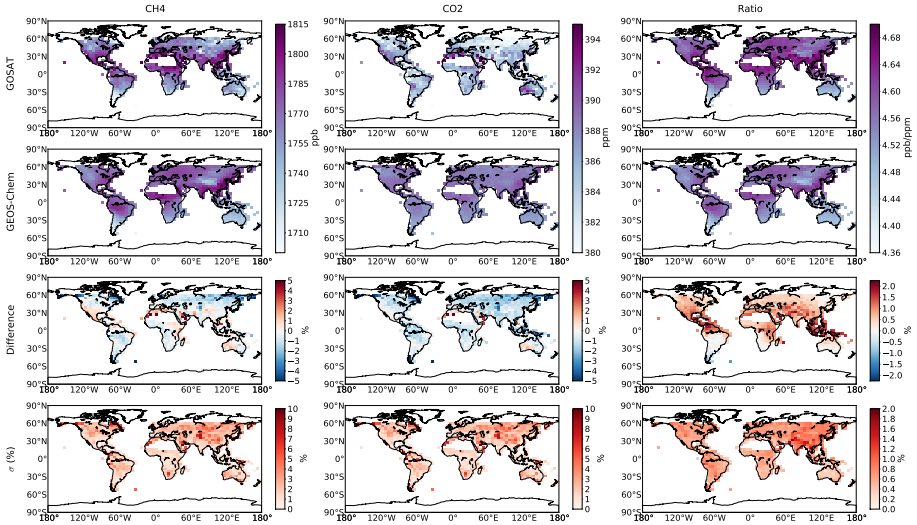

Figure 4. Annual mean GOSAT (top row) and GEOS-Chem model (second row) XCH_4, XCO_2, and $XCH_4 : XCO_2$ ratio measurements from GOSAT during 2010 averaged on the model $4^\circ \times 5^\circ$ grid. The third row shows the percentage difference between them (GOSAT minus GEOS-Chem). For XCH_4 and XCO_2, we truncate at the mean $\pm$ 2-σ. The bottom row shows the 1-σ value in the difference as a percentage about the mean GOSAT XCH_4, XCO_2, and $XCH_4 : XCO_2$ data. The model has been sampled at the time and location of the GOSAT observations, and convolved with scene-dependent averaging kernels.

ACPD
14, 15867–15894, 2014

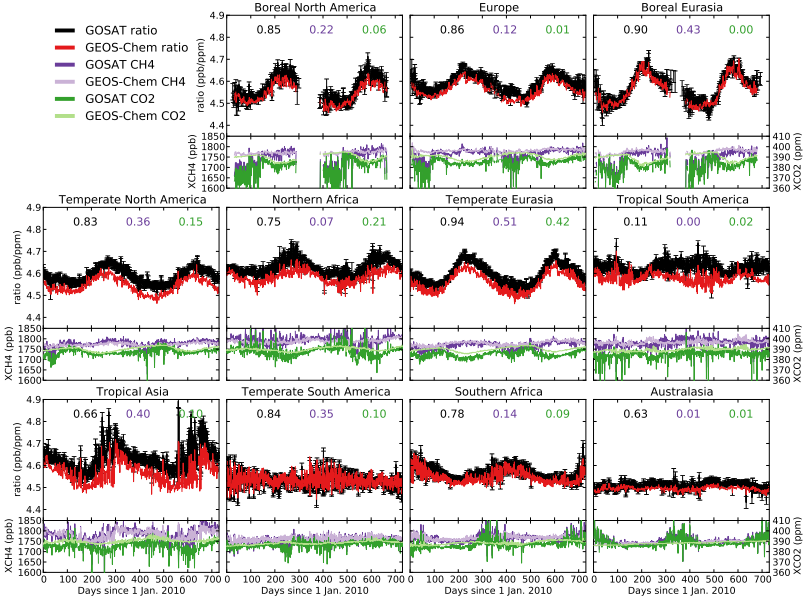

Figure 5. GOSAT and GEOS-Chem daily mean $XCH_4 : XCO_2$ ratios (top panels) for 2010–2011, averaged over each land region shown in Fig. 1. Squared Pearson correlation coefficients between GOSAT and GEOS-Chem are shown inset for the ratio (black), XCH_4 (purple), and XCO_2 (green). Bottom panels show the corresponding GOSAT and GEOS-Chem daily mean XCH_4 and XCO_2. The model has been sampled at the time and location of the GOSAT observations, and convolved with scene-dependent averaging kernels.

ACPD
14, 15867–15894, 2014

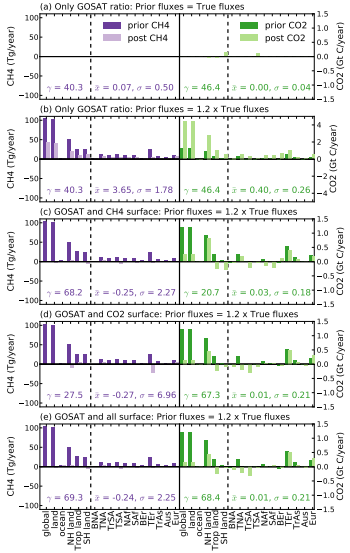

Figure 6. Regional flux estimates of CH_4 (left) and CO_2 (right) inferred from various observing system simulation experiments, where values are described as the departure from the corresponding true flux. The first six regions are aggregates: global represents all regional fluxes; land omits the oceans and vice versa; NH land sums fluxes from Boreal and Temperate North America, Europe, and Boreal and Temperate Eurasia; Trop land sums fluxes from Tropical South America, Northern Africa, and Tropical Asia; and SH land sums fluxes from Temperate South America, Southern Africa, and Australasia. The remaining regions are defined in Fig. 1. Experiment **(a)** for which the a priori and the truth are the same and only GOSAT data are used; experiment **(b)** is as **(a)** but the a priori fluxes are 20 % higher than the truth; experiment **(c)** is as **(b)** but CH_4 surface flask data are also used; experiment **(d)** is as **(b)** but CO_2 surface flask data are also used; experiment **(e)** is as **(b)** but CH_4 and CO_2 surface flask data are also used. Note the different y-scale for CO_2 in **(b)**. The error reduction in the global fluxes (γ), the mean ($\overline{x}$) and standard deviation (σ) of the difference in the individual regions are shown inset of each panel.

ACPD
14, 15867–15894, 2014

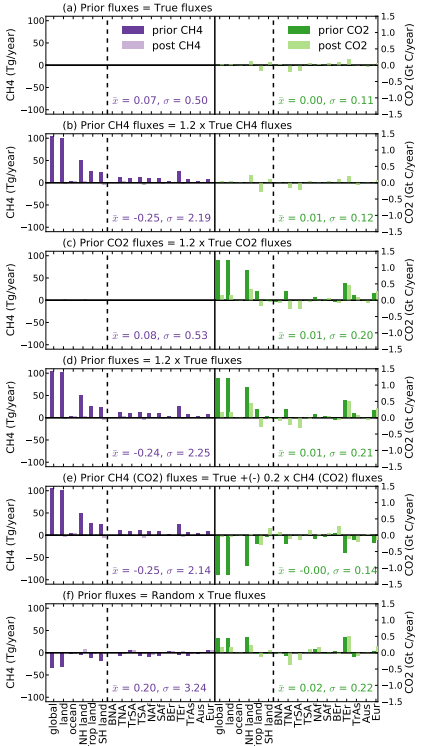

Figure 7. As Fig. 6 but all experiments use CH_4 and CO_2 surface flask data and GOSAT data. Experiment **(a)** for which a priori fluxes are equal to the true fluxes; experiment **(b)** for which CH_4 a priori fluxes are 20 % larger than the true fluxes; experiment **(c)** for which CO_2 a priori fluxes are 20 % larger than the true fluxes; experiment **(d)** for which CH_4 and CO_2 a priori fluxes are 20 % larger than their true fluxes; experiment **(e)** for which CH_4 a priori fluxes are 20 % larger and CO_2 a priori fluxes are 20 % smaller than their true fluxes; and experiment **(f)** for which all a priori fluxes are perturbed stochastically, ranging from −20 % to 20 %, from the true fluxes.

ACPD
14, 15867–15894, 2014

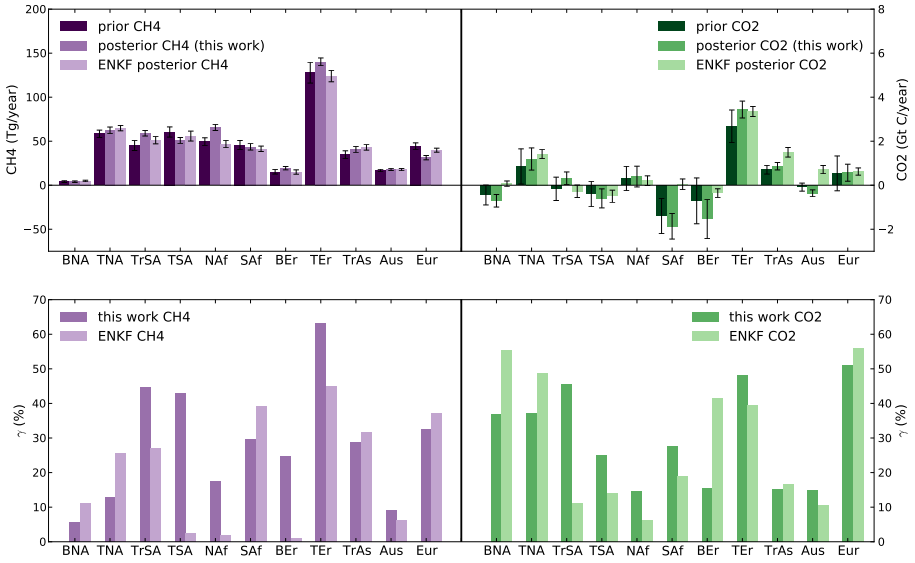

Figure 8. A priori and a posteriori CO_2 and CH_4 regional land fluxes inferred from GOSAT $XCH_4 : XCO_2$ and surface measurements of CO_2 and CH_4 and from XCO_2 or XCH_4 using an ensemble Kalman filter (top) (Feng et al., 2011; Fraser et al., 2013), and the corresponding reduction in uncertainty (bottom), during 2010. Error bars atop of emission estimates represents the 1-σ uncertainty.

ACPD
14, 15867–15894, 2014